Control of cavitating flow over a 2D hydrofoil by active mass injection through a slot channel in its surface

Timoshevskiy, Mikhail V.; Pervunin, Konstantin S.; Markovich, Dmitriy M.; Hanjalić, Kemal

Publication date
2019

Document Version
Final published version

Published in
Open Archives of the 16th International Symposium on Transport Phenomena and Dynamics of Rotating Machinery, ISROMAC 20162019

Control of cavitating flow over a 2D hydrofoil by active mass injection through a slot channel in its surface

Mikhail Timoshevskiy, Konstantin Pervunin, Dmitriy Markovich, Kemal Hanjalić

Control of cavitating flow over a 2D hydrofoil by active mass injection through a slot channel in its surface

Mikhail V. Timoshevskiy[1,2], Konstantin S. Pervunin[1,2]*, Dmitriy M. Markovich[1,2,3], Kemal Hanjalić[2,4]

ISROMAC 2016

International Symposium on Transport Phenomena and Dynamics of Rotating Machinery

Hawaii, Honolulu

April 10-15, 2016

Abstract

We studied cavitating flow over the suction side of a symmetric 2D foil – a scaled-down model of high-pressure hydroturbine guide vanes (GV) – in different cavitation regimes at several attack angles. High-speed imaging was used to analyze spatial patterns and time dynamics of the gas-vapor cavities, as well as for evaluating the characteristic integral parameters. A hydroacoustic pressure transducer was employed to register time-spectra of pressure fluctuations behind the hydrofoil and, thereby, determine dedicated frequencies of unsteady regimes. A PIV technique was applied to measure the velocity fields and its fluctuations, which were compared for the free and forced flow conditions. The active flow control was implemented by means of a continuous liquid supply with different flow rates through a slot channel located in the GV surface at the distaence of 60% of the chord length from the foil leading edge. It was found that the active mass injection does not influence the primary flow upstream of the slot channel position absolutely. At small angles of incidence, the injection flow at velocities in the range between zero to 0.76 of the mean bulk velocity was observed not to practically influence the distributions of turbulent characteristics so that the global difference is only between the free and forced flow conditions. For cavitation-free and cavitation inception cases, the active mass injection was shown to make the flow turbulence structure more developed and the wake past the GV section more intense. However, the active flow control system considered also allows a favorable and efficient flow manipulation, especially at the regimes with developed gas-vapor cavities. Moreover, the active flow management makes it possible to reduce substantially the amplitude or totally suppress the periodic cavity length oscillations and pressure pulsations associated with them.

Keywords

Cavitation, partial cavities, flow control, active mass injection, high-speed imaging, PIV, guide vane modell

[1] *Kutateladze Institute of Thermophysics, Siberian Branch of the Russian Academy of Sciences, Novosibirsk, Russia*

[2] *Department of Scientific Research, Novosibirsk State University, Novosibirsk, Russia*

[3] *Institute of Power Engineering, Tomsk Polytechnic University, Tomsk, Russia*

[4] *Department of Chemical Engineering, Delft University of Technology, Delft, the Netherlands*

*__Corresponding author__: pervunin@itp.nsc.ru

INTRODUCTION

Unsteady cavitation phenomena occurring within the ducts of real hydropower systems (especially, on guide vanes, runner blades and in draft tubes of hydroturbines) are known to be one of the main sources of instabilities that cause significant vibrations, overloads and, consequently, fatigue damages. These might lead to unstable operating conditions, reduced efficiency and safety problems. Therefore, in full-scale conditions all types of instabilities are typically suppressed as much as possible. Apart from omnipresent erosion, cavitation is not regarded as dangerous as long as its dynamics is stable. Preventing or at least diminishing and controlling cavitation and other causes of instabilities in full-scale hydropower systems is nowadays a vital and relevant problem.

Presently, two main classes of partial cavity instabilities are distinguished [1]: intrinsic and system. If instability originates in the cavity itself, it is of intrinsic type. If it is caused by interaction of the cavity with other cavities or elements of the hydraulic system, especially inlet and outlet ducts, it is system dependent. For example, cloud cavitation occurs because of the development of an intrinsic instability – a re-entrant jet underneath the sheet cavity (e.g., see [2–4]). The thickness of the re-entrant jet and its velocity are determined by an adverse pressure gradient. If the pressure gradient is strong enough to force the re-entrant jet to impinge upon the cavity detachment region (i.e., close to the cavity leading edge), the attached cavity interface breaks up over the whole foil span and a cloud cavity appears, which is then convected downstream by the primary flow.

The most general case of system instabilities is the so-called cavitation surge that prevails for relatively long and thin cavities (typically when the cavity length is about 75-100% of a foil chord) on hydrofoils [1, 5, 6]. According to Callenaere et al. [1], the mechanism of this instability is as follows. A minor pressure drop at a cavity location makes its volume increase and, as a result, hydraulic resistance grows. In order to counterbalance this, the flow decelerates at the inlet duct, which makes the local pressure gradually grow and the cavity volume decreases. When the cavity reaches its minimum length, local velocity on the contrary increases maximally that leads again to a local pressure drop. Afterwards, the process repeats and the system as a whole oscillates at a certain frequency. Thus, when cavitation surge conditions are fulfilled, the mechanism of the cavity length pulsations is driven by propagation of pressure waves along the test channel.

The control of cavitation inception and development, its suppression or avoidance can be achieved by both the active and passive methods. Presently, there are several promising approaches of active management of cavitating flow based on different underlying principles. The most prevailing are the control of cavitation nuclei by means of ultrasound or electrolysis (e.g. [7, 8]), injection or suction of basic fluid or various solutions through a body surface [9] and forced transition of a boundary layer to turbulence by imposing external oscillations or vibrations [10]. In all passive methods cavitation manipulation is implemented by means of changing the wall properties in one or another way. These are selection of the surface material with certain characteristics [11], creation of irregular [12] or distributed [13, 14] roughness and application of compliant coatings [15].

The paper aims at the investigation of partial cavity flows around a scaled-down model of guide vanes (GV) of a high-pressure turbine at different attack angles and cavitation numbers and control of the cavitation by means of continuous mass injection through a spanwise slot channel in the foil surface. We report here on high-speed visualization of spatial structure and dynamics of attached and cloud cavities and their integral characteristics, a comparison of frequency spectra of pressure pulsations near the profile made by a hydrophone and PIV measurements of the spatial distributions of the mean velocity and its turbulent fluctuations around the cavitating GV model.

1. EXPERIMENT

The experiments were carried out in the Cavitation tunnel in Kutateladze Institute of Thermophysics SB RAS. Its description as well as details on the experimental conditions and measurement techniques applied can be found in [16]. Cavitation number $\sigma = (P_{in} - P_V)/(\rho U_0^2/2)$, where P_{in} and P_V are the static pressure at the test section inlet and the water vapor pressure, respectively, ρ is water density and U_0 is the mean (bulk) flow velocity, was controlled by varying the mean flow velocity, which was chosen to achieve a range of targeted cavitation regimes. Three attack angles have been considered in tests, α = 0, 3 and 9°.

The test foil of C = 100 mm chord length was a scaled-down model of a Francis turbine guide vane (GV), which is a two-dimensional body (Figure 1 and Table 1), with a blunt trailing edge of 1.31 mm height. It was made of brass with the mean surface roughness of 1.5 μm. The maximum width of GV is H_{max} = 0.2206C measured at the distance of x_{max} = 0.4396C from the leading edge. The GV rotating axis is slightly shifted to its trailing edge and is located at the distance of 0.54C from the foil leading edge. The aspect ratio (the ratio of the foil span to its chord) was AR = 0.8 that is very close to the one in some practical full-scale conditions.

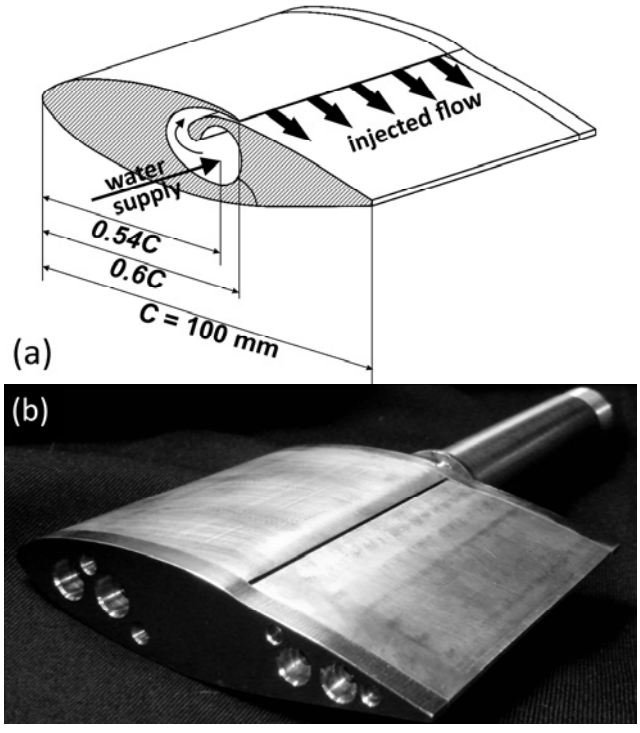

Figure 1. (a) A 3D scheme and (b) photograph of the fabricated GV profile.

In order to provide the flow control, the hydrofoil was manufactured with a spanwise slot channel in its surface (Figure 1) through which the liquid from a bypass circuit was supplied directly to the test section along the GV surface. The slot nozzle exit of 0.6 mm height and 70 mm width was located at the distance of 0.6C from the foil leading edge so that the liquid was

injected across the whole foil span, except for the end caps of 5 mm width. The height of the backward facing step formed by the slot and its wall was 0.8 mm. The nozzle chamber inside the GV profile had a helical geometry with a contraction towards the exit (Figure 1-a).

Table 1. Points of the generatrix of the guide vane model at different cross-sections. y_{up} and y_{down} are the transversal coordinates of these points at the upper (with slot) and lower (w/o slot) surfaces with respect to the foil chord (zero line). The GV thickness $H(x) = y_{up} - y_{down}$. The GV shape is a result of a cubic spline approximation of these values.

x/C	y_{up}/C	y_{down}/C
0	0	0
0.1	0.0658	–0.0658
0.2	0.0898	–0.0898
0.3	0.1045	–0.1045
0.4	0.1098	–0.1098
0.5	0.1087	–0.1087
0.6	0.0921 / 0.0850	–0.0981
0.7	0.0713	–0.0792
0.8	0.0544	–0.0554
0.9	0.0312	–0.0312
1	0.0065	–0.0065

The injected liquid was delivered into the nozzle chamber through a channel of 13 mm inner diameter in the hydrofoil axis by a pump or owing to the pressure gradient. The maximum flow rate through the slot channel was 0.44 l/s, which corresponded to the maximum velocity of the slot wall jet U_{in} = 10.6 m/s. The measurement uncertainty of the injection velocity was 0.2 m/s. In the branch circuit, the liquid was taken close to the centrifugal pumps of the main facility loop and was partly supplied to the test section and the rest of it was returned via a bypass line back into the facility so that the total liquid volume was constant.

In tests, local pressure measurements were also carried out near the GV foil by means of a hydroacoustic pressure transducer – a hydrophone Brüel&Kjær Type 8103 (the sensor diameter – 9.5 mm, sensitivity – 24.6 μV/Pa, frequency spectrum – from 0.1 Hz to 180 kHz, resolution accuracy – +1.5 dB for 0.1 Hz and –6 dB for 100 kHz) – that was flush-mounted into the sidewall of the test section. It was positioned at the center of the test section in the vertical direction and 80 mm shifted behind the GV trailing edge. The sidewall at which the hydrophone was fixed is a black-colored duralumin plate of 10 mm width that is vibrationally isolated by rubber pads from the resting part of the test section and the experimental facility as a whole.

The velocity fields were measured by a ‘‘POLIS’’ PIV-system consisting of a double-pulsed Nd:YAG Quantel EVG00200 laser (wavelength 532 nm, repetition rate 15 Hz, pulse duration 10 ns, pulse energy 200 mJ), a ImperX B2020 CCD-camera (14 bits per pixel, matrix resolution 2048x2048 pixels) equipped with Nikon AF Nikkor 50 mm f/1.4D lens and an optical low-pass filter (bandpass edge at 570 nm), as well as a synchronizing processor. The PIV-system was operated via a computer using ‘‘ActualFlow’’ software. The current measurements were carried out at the sampling rate of 4 Hz. The thickness of the laser light sheet formed by a cylindrical lens to illuminate tracer particles was about 0.8 mm in the measurement plane that coincided with the central longitudinal plane of the test section parallel to its larger sidewalls. The distance between the camera and the laser sheet was 574 mm. The size of the measurement area was approximately 124x124 mm. Since in a cavitating flow the micro-size vapor bubbles can act as tracers, their contaminating effect on the PIV measurements was reduced by adding fluorescent tracers (average size 10μm, wavelength range 550–700 nm) into the working liquid.

In order to enhance the quality of the registered images, the data were subjected to a two-step pre-processing. First, the mean two-frame intensity field over 5000 initial image pairs was subtracted from each image pair. This allows to compensate the nonuniformity of the image exposure, independently for the first and second frames, as well as to remove glares and shadows in the images. As a result, the intensity of both frames becomes quite similar, improving the accuracy of the velocity vectors calculation in further processing. Secondly, all image pairs were masked to remove from the calculations the areas corresponding to the foil and the shadow.

The velocity fields were calculated using the iterative cross-correlation algorithm with a continuous window shift and deformation and 75% overlap of the interrogation windows. In addition, during the correlation step the local particle image concentration was accounted for in the correlation analysis only in those interrogation areas where the particle concentration level is above the given number of particles. The threshold value for seeding particles concentration was set to be 5 tracers per 32x32 pixel area. The tracers were regarded as the convolution of a Gaussian mask with 1 pixel radius and initial image over 5x5 pixels window, with the correlation threshold being 0.7. The sub-pixel interpolation of a cross-correlation peak was performed over three points, using one-dimensional approximation by the Gaussian function. In order to have a relatively large dynamic range (the span between the maximum and minimum velocity), the initial size of the interrogation window was chosen to be 64x64 pixels, but it was subsequently reduced so that the final interrogation window was 8x8 pixels, which provided high enough spatial resolution. The obtained instantaneous velocity vector fields were validated with the three procedures applied successively: the peak

validation with the threshold 2.0, the adaptive median filter over 7x7 nodes and the cluster validation with the coefficient of 50 (for more details refer to [16]).

2. RESULTS AND DISCUSSION

We present below some results of the experimental investigation of cavitating flows over the GV foil for two attack angles, α = 3° and 9° at different regimes defined by the cavitation number. The presentation begins with a discussion of selected images from high-speed visualization and measured pressure fluctuations, followed by distributions of the mean velocity and the rms of the streamwise velocity fluctuations.

2.1. Visualization and pressure measurements

At α = 3°, cavitation is initiated right behind the leading edge on the suction side of the GV profile in form of traveling bubbles (Figures 2-a.1 and 2-a.2). At σ = 0.95, initially transitional cavity that is characterized by relatively small clouds (compared to cloud cavitation regimes) shedding from the cavity closure region is transformed to a typical traveling bubble cavitation as soon as the injection through the slot is started. This leads to a decrease in the dimensions of the cavitation area on the GV surface. However, pressure fluctuations for both cases are almost identical and reveal no effect of injection (Fig. 2-a.3). This influence detected visually is probably linked with the existence of a shear layer past the backward facing step produced by the slot and its wall, which leads to an abrupt reduction of the shear stresses once the injection begins. Weakened shear stresses cannot anymore produce strong spanwise vortices (like in the case without injection) in the centers of which an intense evaporation occurs and, thus, cavitation is suppressed.

When the cavitation number is slightly decreased down to 0.89, the partial cavity on the GV section becomes unsteady and starts to oscillate periodically in the free flow case (Figure 2-b.1). This is also proved by the pressure measurements. The main maximum that is clearly seen in Figure 2-b.3 at St = fC/U_0= 0.21 corresponds to the frequency of the attached cavity pulsations. At this regime, liquid injection results in stabilization of the attached cavity dynamics (Figure 2-b.2), changing the partial cavity regime to transitional one like that shown in Figure 2-a.1. At the same time, the peak in the pressure fluctuations spectrum at St = 0.21 vanishes completely (Figure 2-b.3). When the cavitation number is further reduced to σ = 0.84, the active mass injection does not already change the cavity unsteady behavior (Figures 2-c.1 and 2-c.2) but the amplitude of the pressure pulsations diminishes about three times (cf. the peak heights in Figure 2-c.3).

For a higher incidence angle α = 9°, the injection influence is less pronounced. At some regimes (e.g. see Figure 3), the active flow control has no influence on the cavity characteristics and dynamics, though under certain conditions cavitation area becomes shorter and flow dynamics change (Figures 3-a.1 and 3-a.2). Moreover, the injection sometimes leads to a reverse effect – an increase in pressure fluctuations, for example in Figure 3-a.3 a peak appears at St ≈ 0.07. This occurs when the flow rate through the slot is too low. In such a case, the auxiliary flow is choked periodically because its momentum is sufficient to overcome the adverse pressure gradient only in those moments when the pressure inside the nozzle chamber becomes higher than that at the GV trailing edge. Otherwise, the flow through the slot is blocked for a while.

2.2. Velocity distributions

Figures 4 and 5 display selected profiles of the streamwise component of the time-averaged velocity (plotted as the normalized velocity defect, $(U - U_0)/U_0$) and the rms of the streamwise component of its turbulent fluctuations $\tilde{u}$ at several locations along the GV model. In order to facilitate a direct comparison, the profiles are plotted jointly for free and forced flow conditions only for α = 3° as at this attack angle the injection effect is more pronounced. Typical attached cavity interfaces (obtained from visual data) for the developed cavitation regimes are depicted in the figures as solid and dashed lines for the free and forced flow conditions, respectively. The reference point (the origin of coordinate axes) coincides with the leading edge of the GV section in the measurement plane at α = 0°.

As seen, the injection does not affect the profiles of the mean and fluctuating velocities upstream of the slot channel position at all (cf. the profiles at sections x/C = 0.1 and 0.4 in Figures 4 and 5). Moreover, the injection flow rate corresponding to the range of the injection velocities from U_{in}/U_0 = 0 to 0.76 was found not to practically influence the distributions of these characteristics at α = 3° (not shown in the images) so that the global difference is only between the free and forced flow conditions. Thus, below only these two cases are considered, without taking into account the values of U_{in}/U_0.

For the single-phase flow (Figure 4-a), the injection leads to a decrease in the mean velocity just above the foil trailing edge (x/C = 1) from U/U_0 = 0.41 down to 0.15 ($\Delta U/U_0$ = 0.26). Besides, in the GV wake (x/C > 1) a double growth of the turbulent velocity fluctuations up to $\tilde{u}/U_0$ = 0.23 occurs at the distance of y/C = 0.024 from the GV surface when the injection is started (Figure 5-a), while their amplitude remains almost the same close to the wall. In case of traveling bubble cavitation at σ = 1.06 (Figures 4-b and 5-b), the active mass injection causes the cavitation disappearance and the profiles of

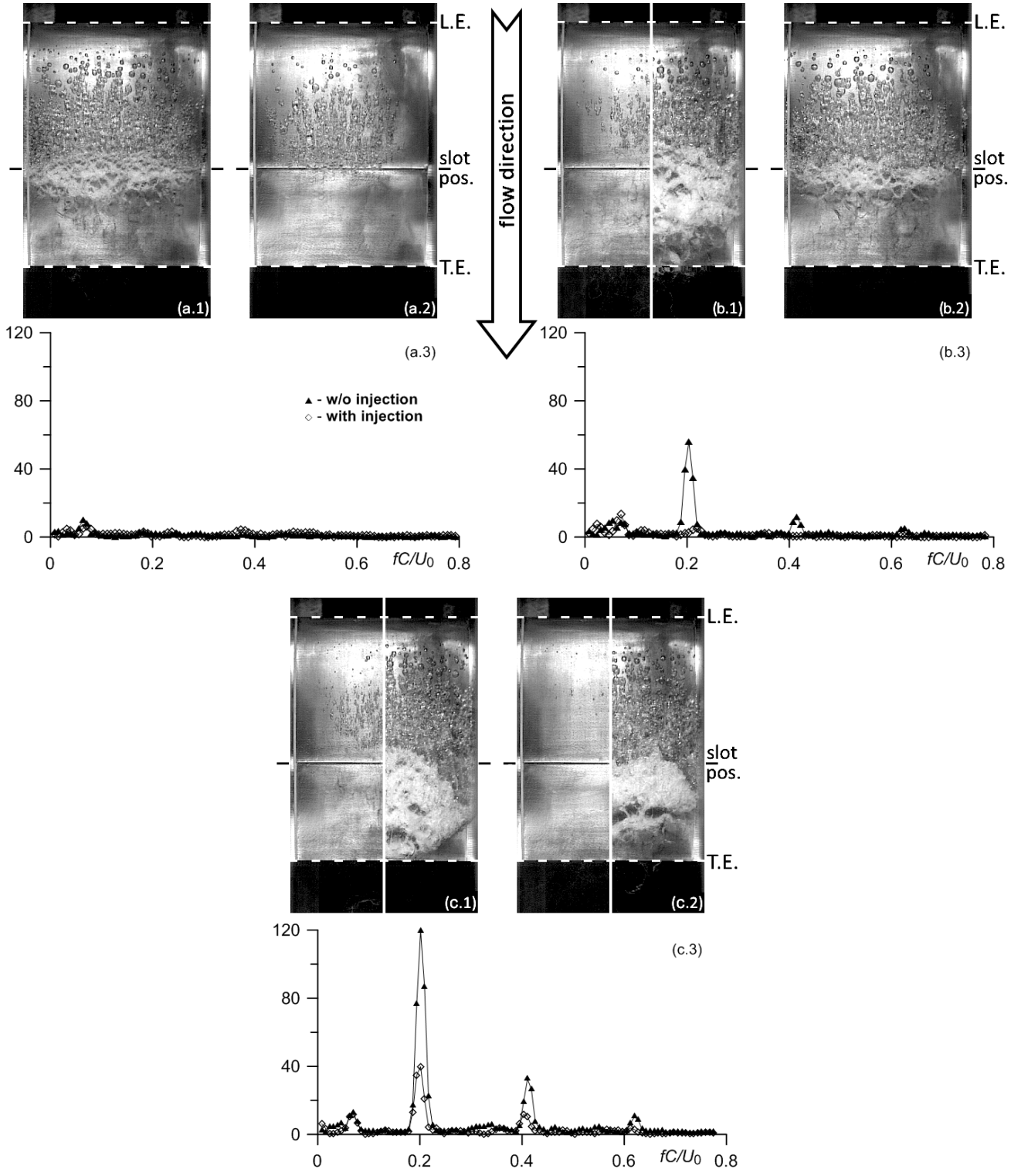

Figure 2. Instantaneous images of partial cavities (top view) on the suction side of the GV model at α = 3° (1) without and (2) with mass injection through the slot channel and (3) comparison of the spectra of pressure fluctuations measured by the pressure transducer for the same flow conditions when: (a) σ = 0.95, U_{in}/U_0 = 0.79 (transitional cavitation/traveling bubbles), (b) σ = 0.89, U_{in}/U_0 = 0.74 (unsteady cavity/ transitional cavitation) and (c) σ = 0.84, U_{in}/U_0 = 0.8 (unsteady cavitation in both cases). For unsteady regimes, half-images indicating the phases of the attached cavity evolution when it has (left) the shortest (just before its detachment) and (right) maximal lengths are shown together.

the mean and fluctuating velocities at x/C = 1 become quite close to each other. The one for the free flow remains unchanged, whereas that for the forced flow is accompanied by a reduction of the fluctuations amplitude (Figure 5-b) and approaches the former. However, at this regime the velocity fluctuations are still higher for the forced flow conditions compared to the

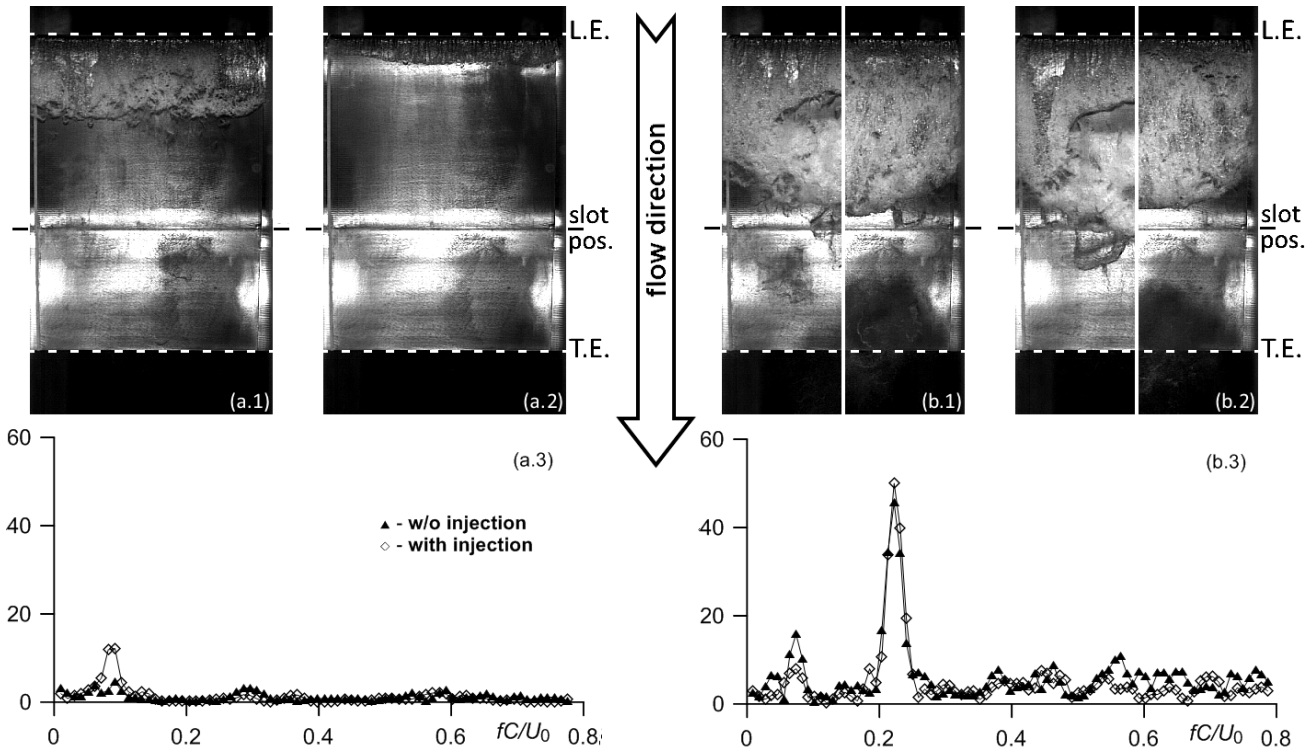

Figure 3. Instantaneous images of partial cavities (top view) on the suction side of the GV model at α = 9° (1) without and (2) with mass injection through the slot channel and (3) comparison of the spectra of pressure fluctuations measured by the pressure transducer for the same flow conditions when: (a) σ = 2.11, U_{in}/U_0 = 0.27 (transitional cavitation/sheet cavity) and (b) σ = 1.61, U_{in}/U_0 = 0.65 (unsteady cavitation in both cases). For unsteady regimes, half-images indicating the phases of the attached cavity evolution when it has (left) the shortest (just before its detachment) and (right) maximal lengths are shown together.

free flow ones. Thus, for these two flow regimes the active mass injection makes the flow turbulence structure more developed and the wake past the GV section more intense.

Transitional cavitation (Figure 4-c) causes substantial changes in the velocity distributions for the free flow conditions. The boundary layer thickness increases from 0.03C at x/C = 0.7 and 0.06C at x/C = 1 (cavitation-free and cavitation inception cases, Figure 4-a and b) up to 0.04C and 0.09C at the same sections, respectively. The mean velocity is noticeably reduced in the near-wall region (y/C < 0.05) in comparison with those for higher cavitation numbers so that its minimum reaches 0.43U_0 at x/C = 0.7 and 0.28U_0 at x/C = 1. Turbulent fluctuations at the same time grow within the boundary and mixing layers up to $\tilde{u}/U_0$ = 0.21 at x/C = 0.7 and 0.17 at x/C = 1. The mass injection results in the modification of the cavitation pattern to traveling bubbles, a decrease of the boundary layer thickness to 0.011C at x/C = 0.7 and 0.035C at x/C = 1 and a reduction of the velocity fluctuations down to $\tilde{u}/U_0$ = 0.14 at x/C = 0.7 and their equalization about the value of $\tilde{u}/U_0$ = 0.2 at x/C = 1 for the same cavitation number σ = 0.95. Consequently, at the regimes of transitional cavitation the active flow control system allows a favorable and efficient flow manipulation.

When transition to unsteady regimes occurs (Figure 4-d and e), the boundary layer widens up to 0.07C at x/C = 0.7 and 0.14C at x/C = 1 for the free flow conditions. The mass injection does not, however, influence the transversal size of the boundary layer but somewhat reduces the mean flow velocity inside it. So, close to the wall $\Delta U/U_0$ reaches 0.3 at x/C = 0.7 and 0.1 at x/C = 1 for σ = 0.89 and 0.2 and 0.16 in the same cross-sections for σ = 0.84 (see Figure 4-d and e). In addition, under the forced conditions, the turbulent fluctuations are in general lower (typically about 0.08U_0) in comparison with the free flow conditions. Further, the active flow management makes it possible to totally suppress the periodic cavity length oscillations for certain conditions as for instance in the case of σ = 0.89 (Figures 4-d and 5-d). Hence, the continuous liquid supply through a slot channel in the GV section surface is an effective tool for flow management.

CONCLUSIONS

High-speed visual imaging and PIV velocity measurements provided information on the main features of the cavitation incipience and development, the cavity spatial structure and its dynamics, as well as distributions of the mean and turbulent characteristics of the flow over a modified scaled-down model of symmetric guide vanes of high-pressure turbines (GV)

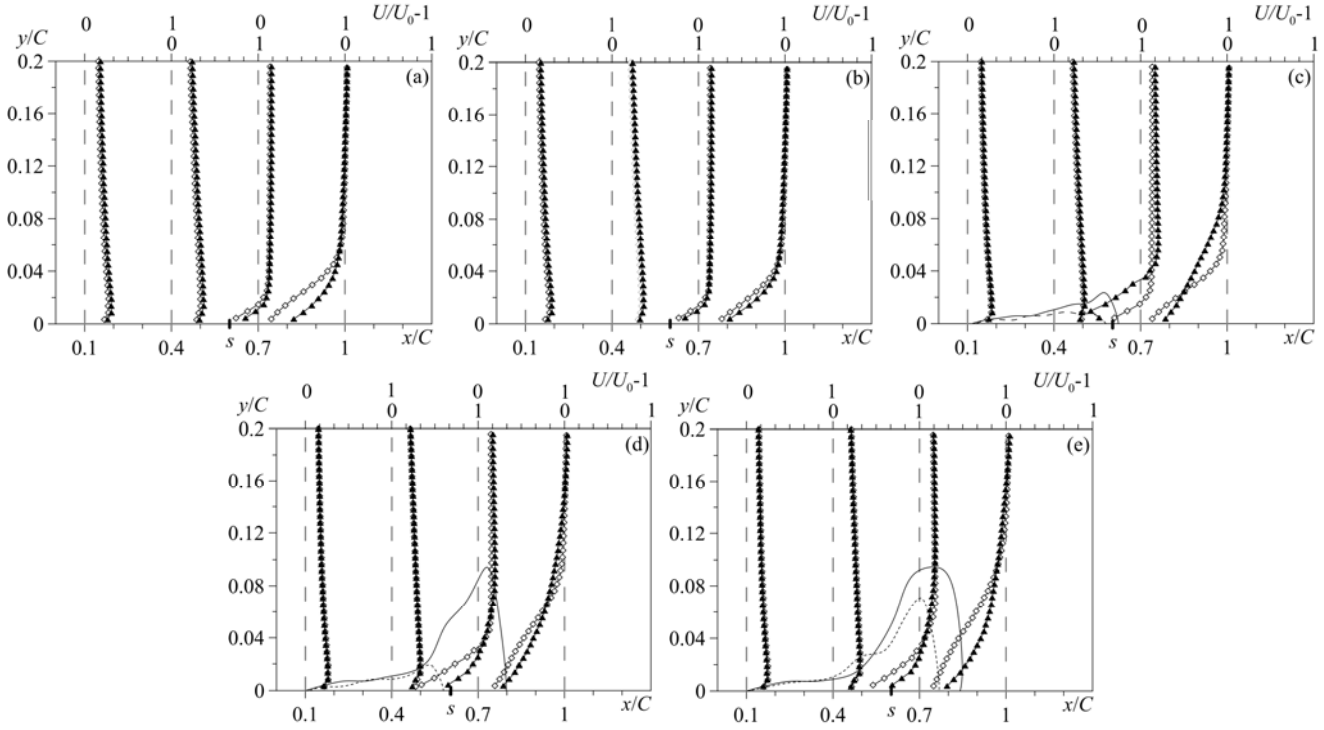

Figure 4. Downstream evolution of the streamwise component of the mean velocity over the suction side of the GV model for (a) cavitation-free flow at σ = 1.3, U_{in}/U_0 = 0.65; (b) traveling bubbles/cavitation-free flow at σ = 1.06, U_{in}/U_0 = 0.65; (c) transitional cavitation/traveling bubbles at σ = 0.95, U_{in}/U_0 = 0.66; (d) unsteady cavity/transitional cavitation at σ = 0.89, U_{in}/U_0 = 0.74 and (e) unsteady cavitation in both cases at σ = 0.84, U_{in}/U_0 = 0.76. α = 3°. ▲ – w/o injection, ◇ – with injection. Solid and dashed lines represent interfaces (extracted from visual data) of the attached cavities of maximum size on the GV section for the free and forced flow conditions. *s* denotes the position of the slot channel in the foil surface. The flow direction is from the left.

with a slot spanwise channel in its surface at several attack angles. The results under free flow conditions are compared with those under the forced flow conditions for different cavitation regimes (from single-phase flow to unsteady cavitation).

It was found that the active mass injection does not influence the primary flow upstream of the slot channel position absolutely. At small angles of incidence, the injection flow at velocities in the range between zero to 0.76 of the mean bulk velocity was observed not to practically influence the distributions of turbulent characteristics so that the global difference is only between the free and forced flow conditions. For cavitation-free and cavitation inception cases, the active mass injection was shown to make the flow turbulence structure more developed and the wake past the GV section more intense. Thus, in these cases the use of the injection is undesirable.

However, the active flow control system considered also allows a favorable and efficient flow manipulation, especially at the regimes with developed gas-vapor cavities. Moreover, the active flow management makes it possible to reduce substantially the amplitude or totally suppress the periodic cavity length oscillations and pressure pulsations associated with them. Hence, the continuous liquid supply through a slot channel in the GV section surface is an effective tool for flow management. Unfortunately, the spatial resolution of the performed velocity measurements is insufficient to distinguish the shear layer at the slot position and, therefore, some conclusions made throughout the paper must remain only conjectures so far. This makes it necessary to carry out additional experiments in future with a higher spatial resolution.

ACKNOWLEDGMENTS

The research was funded by a grant from the Russian Scientific Fund (Project No. 14-29-00203) through Novosibirsk State University.

REFERENCES

[1] M. Callenaere, J.-P. Franc, J.-M. Michel and M. Riondet. The cavitation instability induced by the development of a re-entrant jet. *Journal of Fluid Mechanics*, 444: 223–256, 2001.

[2] A. Kubota, H. Kato, H. Yamaguchi and M. Maeda. Unsteady structure measurement of cloud cavitation on a foil section using conditional sampling technique. *ASME Journal of Fluids Engineering*, 111(2): 204–210, 1989.

[3] Y. Kawanami, H. Kato, H. Yamaguchi, M. Tanimura and Y. Tagaya. Mechanism and control of cloud cavitation. *ASME Journal of Fluids Engineering*, 119(4): 788–794, 1997.

[4] T.M. Pham, F. Larrarte and D.H. Fruman. Investigation of unsteady sheet cavitation and cloud cavitation mechanisms. *ASME Journal of Fluids Engineering*, 121(2): 289–296, 1999.

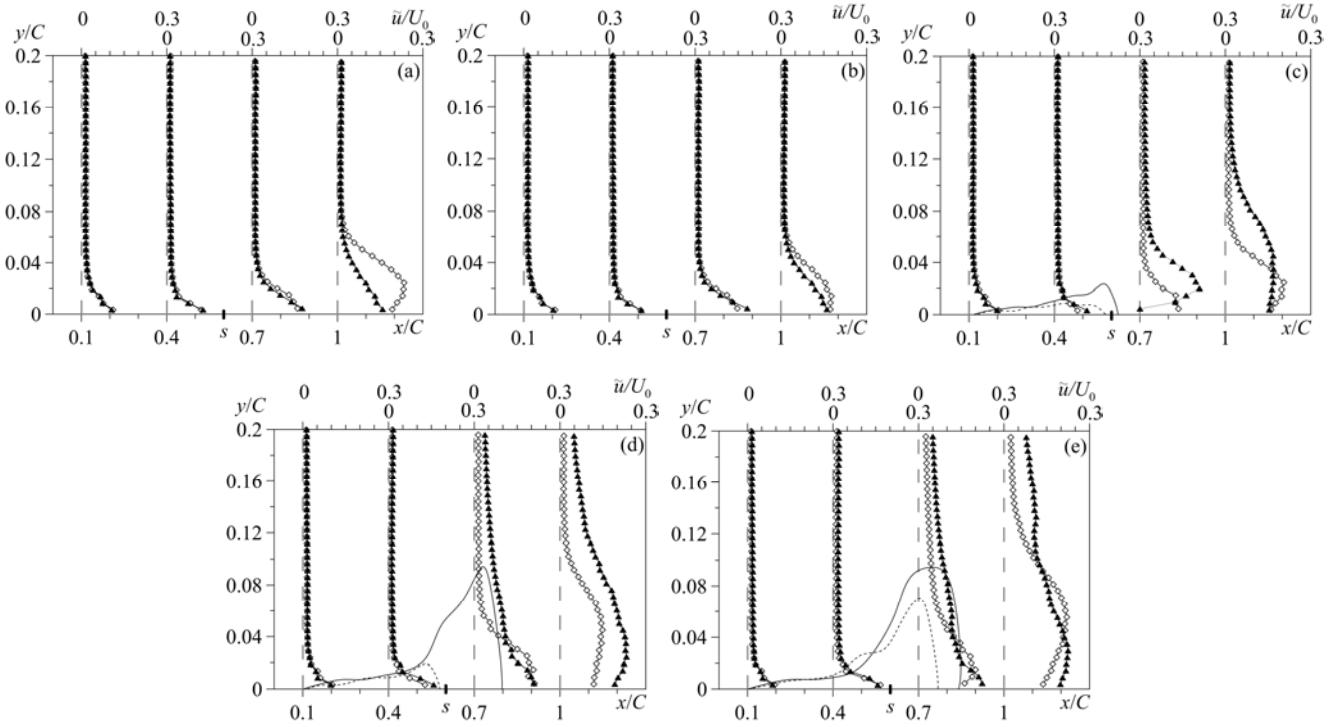

Figure 5. Downstream evolution of the streamwise turbulence intensity (rms-values) over the suction side of the GV model for (a) cavitation-free flow at σ = 1.3, U_{in}/U_0 = 0.65; (b) traveling bubbles/cavitation-free flow at σ = 1.06, U_{in}/U_0 = 0.65; (c) transitional cavitation/traveling bubbles at σ = 0.95, U_{in}/U_0 = 0.66; (d) unsteady cavity/transitional cavitation at σ = 0.89, U_{in}/U_0 = 0.74 and (e) unsteady cavitation in both cases at σ = 0.84, U_{in}/U_0 = 0.76. α = 3°. ▲ – w/o injection, ◇ – with injection. Solid and dashed lines represent interfaces (extracted from visual data) of the attached cavities of maximum size on the GV section for the free and forced flow conditions. *s* denotes the position of the slot channel in the foil surface. The flow direction is from the left.

[5] S. Watanabe, Y. Tsujimoto and A. Furukawa. Theoretical analysis of transitional and partial cavity instabilities. *ASME Journal of Fluids Engineering*, 123(3): 692–697, 2001.

[6] D.T. Kawakami, A. Fuji, Y. Tsujimoto and R.E.A. Arndt. An assessment of the influence of environmental factors on cavitation instabilities. *ASME Journal of Fluids Engineering*, 130(3): (031303)–8, 2008.

[7] D. Chatterjee and V.H. Arakeri. Towards the concept of hydrodynamic cavitation control. *Journal of Fluid Mechanics*, 332: 377–394, 1997.

[8] D. Chatterjee and V.H. Arakeri. Some investigations on the use of ultrasonics in travelling bubble cavitation control. *Journal of Fluid Mechanics*, 504: 365–389, 2004.

[9] N. Chang, H. Ganesh, R. Yakushiji and S.L. Ceccio. Tip vortex cavitation suppression by active mass injection. *ASME Journal of Fluids Engineering*, 133(11): (111301)–11, 2011.

[10] J.P. Franc and J.M. Michel. Unsteady attached cavitation on an oscillating hydrofoil. *Journal of Fluid Mechanics*, 193: 171–189, 1988.

[11] A. Tassin Leger and S.L. Ceccio. Examination of the flow near the leading edge of attached cavitation. Part 1. Detachment of two-dimensional and axisymmetric cavities. *Journal of Fluid Mechanics*, 376: 61–90, 1998.

[12] O. Coutier-Delgosha, J.-F. Devillers, M. Leriche and T. Pichon. Effect of wall roughness on the dynamics of unsteady cavitation. *ASME Journal of Fluids Engineering*, 127: 726–733, 2005.

[13] Y. Kawanami, H. Kato, H. Yamaguchi, M. Tanimura and Y. Tagaya. Mechanism and control of cloud cavitation. *ASME Journal of Fluids Engineering*, 119: 788–794, 1997.

[14] Ph. Ausoni, A. Zobeiri, F. Avellan and M. Farhat. The effects of a tripped turbulent boundary layer on vortex shedding from a blunt trailing edge hydrofoil. *ASME Journal of Fluids Engineering*, 134: (051207)–11, 2012.

[15] D.T. Akcabay, E.J. Chae, Y.L. Young, A. Ducoin and J.A. Astolfi. Cavity induced vibration of flexible hydrofoils. *Journal of Fluids and Structures*, 49: 463–484, 2014.

[16] A.Yu. Kravtsova, D.M. Markovich, K.S. Pervunin, M.V. Timoshevskiy and K. Hanjalić. High-speed visualization and PIV measurements of cavitating flows around a semi-circular leading-edge flat plate and NACA0015 hydrofoil. *International Journal of Multiphase Flow*, 60: 119–134, 2014.